

Frequency Responses of a Graphene Oxide Reinforced Concrete Structure

Respuestas de frecuencia de una estructura de hormigón reforzado con óxido de grafeno

EÍDOS N°24
Revista Científica de Arquitectura y Urbanismo
ISSN: 1390-5007
revistas.ute.edu.ec/index.php/eidos

^{1,2,3,4}Mostafa Habibi, ⁵Mohammad Habibi, ⁶Emad Toghroli, ^{7,8}Maryam Safa, ^{9,10}Morteza Shariati

¹Institute of Research and Development, Duy Tan University, Da Nang 550000, Viet Nam.

²Faculty of Electrical-Electronic Engineering, Duy Tan University, Da Nang 550000, Viet Nam.

³Department of Biomaterials, Saveetha Dental College and Hospital, Saveetha Institute of Medical and Technical Sciences, Chennai, 600 077, India.

⁴Center of Excellence in Design, Robotics, and Automation, Department of Mechanical Engineering, Sharif University of Technology, Azadi Avenue, P.O. Box 11365-9567, Tehran, Iran. mostafahabibi@duytan.edu.vn. ORCID: 0000-0003-1638-0338

⁵Department of Materials and Metallurgy, Faculty of Mechanical and Energy Engineering, Shahid Beheshti University, Tehran, Iran. Mohammad@calut.com.au. ORCID: 0009-0009-0772-5841

⁶Department of Civil Engineering, Calut Company Holding, Melbourne, 800, Australia. emadtoghroli@calut.com.au. ORCID: 0009-0005-3593-5345

⁷Institute of Research and Development, Duy Tan University, Da Nang 550000, Viet Nam.

⁸Faculty of Electrical-Electronic Engineering, Duy Tan University, Da Nang 550000, Viet Nam. maryamsafa@duytan.edu.vn. ORCID: 0009-0003-0535-7447

⁹Department of Civil Engineering, Calut Company Holding, Melbourne, 800, Australia.

¹⁰Department of Civil Engineering Discipline, School of Engineering, Monash University, Melbourne 3800, Australia. mortezashariati@calut.au. ORCID: 0009-0007-0258-0896

Abstract:

This paper presents a comprehensive investigation on the vibrations of reinforced concrete structure by graphene oxide powders (GOPs) using a polynomial displacement field and the Generalized Differential Quadrature Method (GDQM). The study focuses on analyzing the dynamic behavior of the structure and assessing the effects of three different distribution patterns of GOPs on its vibrations. To accurately model the deformation of the pressure vessel, a polynomial displacement field is employed, taking into account the complex geometrical and material properties of the structure. The results highlight the significant influence of the distribution pattern of GOPs on the natural frequencies of the spherical concrete pressure vessel. The analysis reveals that variations in the weight fraction and arrangement of GOPs have a direct

impact on the stiffness and dynamic characteristics of the structure. Specifically, increasing the weight fraction of GOPs generally leads to higher natural frequencies, indicating enhanced structural rigidity. Moreover, the polynomial displacement field and GDQM demonstrate their effectiveness in accurately predicting the vibrations of the reinforced pressure vessel. The combination of these numerical techniques enables efficient and reliable analysis of the dynamic response, allowing for optimization of the design and performance of spherical concrete pressure vessels.

Keywords: Frequency, vibration; GDQM, graphene oxide powders, GDQM, stability.

Resumen:

Este artículo presenta una investigación exhaustiva sobre las vibraciones de estructuras de hormigón armado mediante polvos de óxido de grafeno (GOP) utilizando un campo de desplazamiento polinómico y el Método de Cuadratura Diferencial Generalizada (GDQM). El estudio se centra en analizar el comportamiento dinámico de la estructura y evaluar los efectos de tres patrones diferentes de distribución de GOP sobre sus vibraciones. Para modelar con precisión la deformación del recipiente a presión, se emplea un campo de desplazamiento polinómico, teniendo en cuenta las complejas propiedades geométricas y materiales de la estructura. Los resultados resaltan la influencia significativa del patrón de distribución de GOP en las frecuencias naturales del recipiente a presión de hormigón esférico. El análisis revela que las variaciones

en la fracción de peso y la disposición de los GOP tienen un impacto directo en la rigidez y las características dinámicas de la estructura. Específicamente, aumentar la fracción de peso de los GOP generalmente conduce a frecuencias naturales más altas, lo que indica una mayor rigidez estructural. Además, el campo de desplazamiento polinómico y el GDQM demuestran su eficacia para predecir con precisión las vibraciones del recipiente a presión reforzado. La combinación de estas técnicas numéricas permite un análisis eficiente y confiable de la respuesta dinámica, lo que permite optimizar el diseño y el rendimiento de los recipientes a presión de hormigón esféricos.

Palabras claves: Frecuencia, vibración; GDQM, polvos de óxido de grafeno, GDQM, estabilidad.

1. INTRODUCTION

Spherical structures find various applications across different industries due to their unique properties and benefits. Here are some notable uses of spherical structures in different industrial sectors (L. Lu, Liao, Habibi, Safarpour, & Ali, 2023; S. Lu, Li, Habibi, & Safarpour, 2023; Ma, Chen, Habibi, & Albaijan, 2023; Tang, Wu, Habibi, Safarpour, & Ali, 2023; Y. Wang et al., 2023). Spherical structures, such as spherical tanks or spheres, are commonly used for the storage of liquefied petroleum gas (LPG) and other volatile fluids (Chen & Lin, 2008; Lee, Yoon, Park, & Yi, 2005). The spherical shape allows for even distribution of pressure, resulting in enhanced structural integrity and reduced stress concentration. Spheres are also used in oil refineries and petrochemical plants for storing gases and liquids under high pressure. In addition, these structures play an important role in aerospace applications, primarily in the design of satellites and space exploration vehicles (Ebrahimi, Hajilak, Habibi, & Safarpour, 2019; Ebrahimi, Mohammadi, Barouti, & Habibi, 2019; Ebrahimi, Supeni, Habibi, & Safarpour, 2020; Habibi, Safarpour, & Safarpour, 2020; Hashemi et al., 2019; H Moayedi et al., 2020; Hossein Moayedi, Ebrahimi, Habibi, Safarpour, & Foong, 2020; H Moayedi, Habibi, Safarpour, Safarpour, & Foong, 2019; Mohammadgholiha,

Shokrgozar, Habibi, & Safarpour, 2019; Mohammadi, Lashini, Habibi, & Safarpour, 2019; Oyarhossein et al., 2020; Shariati, Habibi, Tounsi, Safarpour, & Safa, 2020; Shariati, Mohammad-Sedighi, Žur, Habibi, & Safa, 2020; Shokrgozar, Safarpour, & Habibi, 2020). The use of spherical fuel tanks in spacecraft can ensure uniform fuel distribution and stability during maneuvers. In the structure design of the buildings, spherical structures are used in architecture and construction for their aesthetic appeal and structural advantages. Moreover, spherical reactors and vessels are utilized in the chemical and pharmaceutical industry for various processes, such as synthesis, mixing, and containment of reactive substances. Recently, spherical structures find application in renewable energy generation, such as solar power. Solar concentrators, also known as solar spheres, are spherical reflective surfaces used to concentrate sunlight onto a receiver, which then converts it into electricity or thermal energy (Dai, Jiang, Zhang, & Habibi, 2021; Guo et al., 2021; Kong et al., 2022; Z. Liu, Su, Xi, & Habibi, 2020; Shao, Zhao, Gao, & Habibi, 2021; Z. Wang, Yu, Xiao, & Habibi, 2020; Wu & Habibi, 2021; Zhou, Zhao, Zhang, Fang, & Habibi, 2020). In all these applications, spherical structures are subjected to the various loadings from static

to dynamic loading and, hence, structural integrity and strength of such structure is of most important in the design stage.

Although, most of the spherical structures are made from metals and composite materials, there can found examples of construction of spherical vessels using concrete materials (Hamed, Bradford, & Ian Gilbert, 2010; Yan, Wang, Zhai, Meng, & Zhou, 2019; Yue et al., 2022; Zingoni, 2022). Spherical shapes are preferred as they provide optimal volume-to-surface ratio, allowing for efficient accommodation of payloads while minimizing weight and heat transfer. Moreover, concrete are the most used and available materials of construction and demonstrates preferable sustainability and load-carrying capacity.

Novel concretes are usually reinforces with nano-scale materials such carbon nanotubes (CNTs) (Shahpari, Bamonte, & Jalali Mosallam, 2022; Siahkouhi, Razaqpur, Hoult, Hajmohammadian Baghban, & Jing, 2021), graphene platelets (GPLs) (Jaramillo & Kalfat, 2023; Sajjad, Sheikh, & Hadi, 2022) and graphene oxide powders (GOPs) (Cong, Cheng, Tang, & Ling, 2023; Hwangbo et al., 2023; Zeng, Qu, Tian, Hu, & Li, 2023). These nano-materials demonstrated desirable improvement in the concrete properties.

Structural analyses of the concrete structures, as a specific type of composite materials, are widespread. However, one can categorized these analyses in three major categories based on the responses of the structures: static (Godoy, 1987), dynamic (Dong, Li, & Zheng, 2010), stability (Pan & Cui, 2010; J. Zhang et al., 2018) analyses. In the static analysis, the main focus is on the state of displacement and stress distribution of the concrete under static and semi-static loading conditions. In these analyses, deflection of the structure is important to for functionality of the structure and stress information is used to design a superior structure to avoid failure. Mahapatra et al. investigated the large deflection vibration. In the study conducted by Ma-

hapatra et al. (Mahapatra, Kar, & Panda, 2015), the focus was on investigating the behavior of spherical structures made from layer-wise composite materials under large deflection vibrations. Their analysis considered various types of loading, including thermal and moisture loadings. To mathematically model the composite structure, they employed a higher-order shear deformation theory and a general nonlinear form of Green strain definition. By applying Hamilton's principle, they derived the governing equations for the system. The results revealed the significant influence of the composite pattern and geometry on the frequency responses of the spherical structure.

Van Do and Lee (Van Do & Lee, 2020) extended the research by evaluating both static deflection and free oscillation characteristics of spherical and cylindrical composite shell structures reinforced with Glass Fiber Reinforced Polymer (GFRP). They utilized an isogeometric analysis methodology and incorporated different configurations of reinforcement distribution in the laminate composite. The analyses employed Reddy's shell model and Non-Uniform Rational B-Spline (NURBS) curves. The primary focus of their study was to investigate the impact of varying reinforcement distributions on the static and dynamic responses of curved shell structures.

The post-buckling behavior of spherical shells is of great importance in numerous industrial applications. Hutchinson (Hutchinson, 2016) conducted an analytical investigation to explore the post-buckling state in spherical structures using analytical methods. This research aimed to provide insights into the structural behavior and stability of spherical shells following the occurrence of buckling.

Additionally, Ghavanloo et al. (Ghavanloo, Rafii-Tabar, & Fazelzadeh, 2019) introduced the nonlocal theory of elasticity in their analysis of small-size spherical structures subjected to vibrations. The study highlighted that the dynamic response of

small-scale spherical structures differs from that of macro-scale spheres. The incorporation of nonlocal effects allowed for a more comprehensive understanding of the vibration behavior in small-sized structures. Pang et al. (Pang, Li, Chen, & Shan, 2021) examined the effects of boundary conditions on the vibrational behavior of a jointed cylindrical and spherical dome using Rayleigh-Ritz method.

Overall, these studies collectively contribute to advancing our understanding of the behavior of spherical structures made from composite materials under various loading conditions, including large deflection vibrations, static deflections, post-buckling, and small-scale dynamic responses.

The study focuses on analyzing the dynamic behavior of the pressure vessel and assessing the effects of three different distribution patterns of GOPs on its vibrations. To accurately model the deformation of the pressure vessel, a polynomial displacement field is employed, taking into account the complex geometrical and material properties of the structure. The results highlight the significant influence of the distribution pattern of GOPs on the natural frequencies of the spherical concrete pressure vessel. The analysis reveals that variations in the weight fraction and arrangement of GOPs have a direct impact on the stiffness and dynamic characteristics of the structure.

2. METHODOLOGY

2.1. GOP Distribution in Thickness

Figure 1 illustrates an FG-GOPRC spherical structure along with different patterns depicting the distribution of GOPs (Graphene Oxide Polymer Reinforced Composites) in the thickness direction of the spherical shell.

Moving forward, the material properties relevant to this investigation were determined using the Halpin-Tsai homogenization method. This method allows for the estimation of the effective material properties of composite materials, such as the Young's modulus. By employing the Halpin-Tsai approach, we are able to calculate the Young's modulus, which is a key parameter for characterizing the stiffness of the material (Z. Zhang et al., 2020) as follows:

$$E = 0.49 \times \frac{1 + z_L Y_L V_{GOP}}{1 - Y_L V_{GOP}} \times E_m + 0.51 \times \frac{1 + z_t Y_t V_{GOP}}{1 - Y_t V_{GOP}} \times E_m \quad (1)$$

in which, $z_L = z_t = 2 \frac{d_{GOP}}{h_{GOP}}$,

and $Y_t = -\frac{1 - (\frac{\epsilon_{GOP}}{\epsilon_m})}{z_t + (\frac{\epsilon_{GOP}}{\epsilon_m})}$.

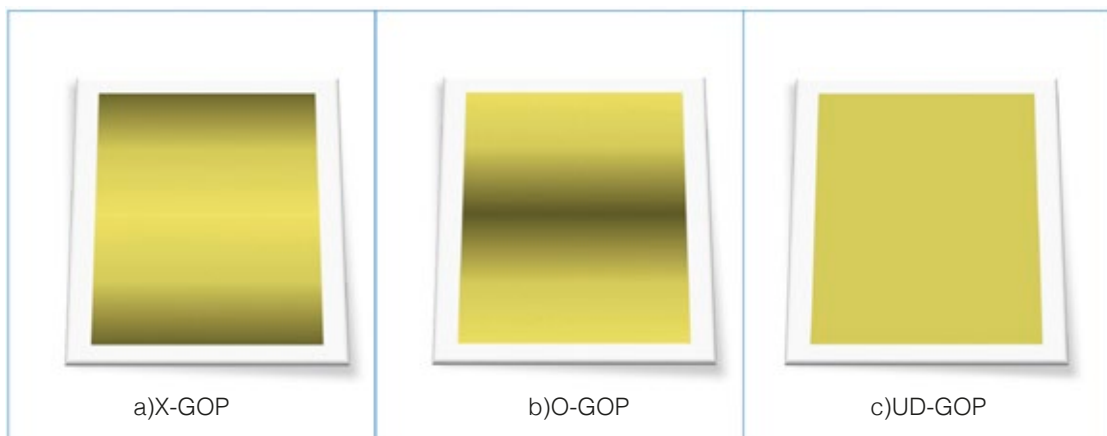


Figure 1. Schematic view of various GPL distribution patterns

In addition to the Young's modulus, the density and Poisson's ratio also considered as follows:

$$\begin{aligned} \rho &= \rho_{GOP} \mathcal{V}_{GOP} + \rho_m (1 - \mathcal{V}_{GOP}), \\ \nu &= \nu_{GOP} \mathcal{V}_{GOP} + \nu_m (1 - \mathcal{V}_{GOP}) \end{aligned} \quad (2)$$

And the shear modulus of the system can be defined as:

$$G = \frac{E}{2(1+\nu)} \quad (3)$$

Lastly, the different pattern of GOPs can be defined as followings for GOP-X (Eq. (4a)), GOP-O (Eq. (4b)) and GOP-UD (Eq. (4c)), (Z. Zhang et al., 2020):

$$\mathcal{V}_{GOP}(k) = 2\mathcal{V}_{GOP}^* \left(\frac{|2k - N_L - 1|}{N_L} \right), \quad (4a)$$

$$\mathcal{V}_{GOP}(k) = 2\mathcal{V}_{GOP}^* \left(1 - \frac{|N_L - 2k + 1|}{N_L} \right), \quad (4b)$$

$$\mathcal{V}_{GOP}(k) = \mathcal{V}_{GOP}^* \quad (4c)$$

Where k changes from 1 layer to N_L .

2.2. Equation of Motion

The displacement field of the spherical shell is expressed by

$$\begin{aligned} R(\vartheta, \theta, Z, t) &= R_0(\vartheta, \theta, t) + \\ &Z R_1(\vartheta, \theta, t) + Z^2 R_2(\vartheta, \theta, t) + \\ &Z^3 R_3(\vartheta, \theta, t) + Z^4 R_4(\vartheta, \theta, t) + \\ &Z^5 R_5(\vartheta, \theta, t), \end{aligned} \quad (5a)$$

$$\begin{aligned} S(\vartheta, \theta, Z, t) &= S_0(\vartheta, \theta, t) + \\ &Z S_1(\vartheta, \theta, t) + Z^2 S_2(\vartheta, \theta, t) + \\ &Z^3 S_3(\vartheta, \theta, t) + Z^4 S_4(\vartheta, \theta, t) + \\ &Z^5 S_5(\vartheta, \theta, t), \end{aligned} \quad (5b)$$

$$\begin{aligned} T(\vartheta, \theta, Z, t) &= T_0(\vartheta, \theta, t) + \\ &Z T_1(\vartheta, \theta, t) + Z^2 T_2(\vartheta, \theta, t) + \\ &Z^3 T_3(\vartheta, \theta, t) + Z^4 T_4(\vartheta, \theta, t) + \\ &Z^5 T_5(\vartheta, \theta, t) \end{aligned} \quad (5c)$$

Where strain displacement can be defined as follows

$$\begin{aligned} g_{\vartheta\vartheta} &= \frac{\partial R}{r \partial \vartheta} + \frac{T}{r}, \quad g_{\theta\theta} = \frac{\partial S}{r_1 \partial \theta} + \frac{R}{r r_1} \frac{\partial R_1}{\partial \theta} + \\ &\frac{T}{r}, \quad g_{ZZ} = \frac{\partial T}{\partial Z}, \\ g_{\vartheta\theta} &= \frac{\partial S}{r \partial \vartheta} - \frac{S}{r r_1} \frac{\partial R_1}{\partial \vartheta} + \frac{\partial R}{r_1 \partial \theta}, \quad g_{\vartheta Z} = \frac{\partial R}{\partial Z} \\ &\frac{R}{r} + \frac{\partial T}{r \partial \vartheta}, \quad g_{\theta Z} = \frac{\partial S}{\partial Z} \frac{S}{r} + \frac{\partial T}{r_1 \partial \theta} \end{aligned} \quad (6)$$

By substituting $r_1 = r \sin \vartheta$ in Eq. (6)

$$\begin{aligned} g_{\vartheta\vartheta} &= \frac{\partial R}{r \partial \vartheta} + \frac{T}{r}, \quad g_{\theta\theta} = \frac{1}{r \sin(\vartheta)} \frac{\partial S}{\partial \theta} + \\ &\frac{\cot(\vartheta) R}{r} + \frac{T}{r}, \quad g_{ZZ} = \frac{\partial T}{\partial Z}, \\ g_{\vartheta\theta} &= \frac{\partial S}{r \partial \vartheta} - \frac{\cot(\vartheta) S}{r} + \\ &\frac{1}{r \sin(\vartheta)} \frac{\partial R}{\partial \theta}, \quad g_{\vartheta Z} = \frac{\partial R}{\partial Z} - \frac{R}{r} + \frac{\partial T}{r \partial \vartheta}, \\ g_{\theta Z} &= \frac{\partial S}{\partial Z} - \frac{S}{r} + \frac{1}{r \sin(\vartheta)} \frac{\partial T}{\partial \theta}. \end{aligned} \quad (7)$$

The unknown quantities in the above equations could be found in (Al-Furjan et al., 2022; Al-Furjan, Oyarhossein, Habibi, Safarpour, & Jung, 2020; Habibi, Mohammedi, Safarpour, Shavalipour, & Ghadiri, 2021; H. Moayedi et al., 2020)

2.3. Hamilton's Principle

The equations that determine motion are derived based on Hamilton's principle:

$$\delta \int_{t_1}^{t_2} (\Pi_k - (\Pi_e + \Pi_w)) dt = 0, \quad (8)$$

Where Π_k , Π_e , and Π_w stand for the kinetic energy, potential energy, and work done by the system respectively. The kinetic energy of the moving plate is indicated as follows

$$\begin{aligned} \Pi_k &= \int_V \frac{1}{2} \rho(\vartheta, \theta, z) \left[\left(\frac{\partial R}{\partial t} \right)^2 + \left(\frac{\partial S}{\partial t} \right)^2 + \right. \\ &\left. \left(\frac{\partial T}{\partial t} \right)^2 \right] dV, \end{aligned} \quad (9)$$

The potential energy of the axially moving plate is illustrated as follows

$$\Pi_u = \int_V \frac{1}{2} [\kappa_{\phi\phi} g_{\phi\phi} + \kappa_{\theta\theta} g_{\theta\theta} + \kappa_{zz} g_{zz} + \kappa_{\theta z} g_{\theta z} + \kappa_{\phi z} g_{\phi z} + \kappa_{\phi\theta} g_{\phi\theta}] dV, \quad (10)$$

The work done by the system:

$$\Pi_u = \int_A \frac{p}{2} \left\{ \frac{1}{r^2 \sin(\phi)} \frac{\partial}{\partial \phi} \left(\sin(\phi) \frac{\partial T_0}{\partial \phi} \right) \right\} + \frac{1}{r^2 \sin^2(\phi)} \frac{\partial^2 T_0}{\partial \phi^2} \right\} T_0 dA, \quad (11)$$

Where P indicates the In-plane mechanical loading. Substituting Eqs. (9), (10), and (11) into Eq. (8), the governing equations of motion and boundary conditions are obtained.

3. SOLUTION PROCEDURE

To illustrate the approximations involved in the Harmonic Differential Quadrature Method (HDQM) using a one-dimensional function, the following equation expresses the p th derivative of $F(\phi)$ in terms of ϕ :

$$\frac{\partial^p \mathcal{F}(\phi)}{\partial \phi^p} = \sum_{j=1}^N \mathcal{G}_{ij}^{(p)} \mathcal{F}(\phi) \quad (12)$$

For $i = 1, 2, \dots, N_\phi$ and $p = 1, 2, \dots, N_\phi - 1$,

here N_ϕ indicates the total number of discrete grid nodes selected through the solution domain.

The equation establishes a relationship between the p th derivative of the function F with respect to ϕ and the variable ϕ itself. This relation serves to demonstrate how the HDQM method approximates the derivatives of a function using a discrete set of values and their corresponding weights. By employing this approach, the HDQM method allows for the efficient and accu-

rate calculation of derivatives in numerical analysis and computational modeling. The term $G_{ij}^{(p)}$ shows the weight coefficients ($j=1, 2, \dots, N_\phi$) at the i th grid-point located in the solution domain. The weight coefficients related to the first-order derivatives $G_{ij}^{(1)}$ for $i \neq j$ would be determined through the following relation:

$$G_{ij}^{(1)} = \frac{\pi P(\phi_i)}{2P(\phi_j) \sin[(\phi_i - \phi_j)/2\pi]}, \quad i, j = 1, 2, \dots, N_\phi, \quad (13)$$

here

$$P(\phi_i) = - \sum_{j=1, j \neq i}^{N_\phi} \sin\left(\frac{\pi(\phi_i - \phi_j)}{2}\right), \quad (14)$$

for $j=1, 2, 3, \dots, N_\phi$.

The weight coefficients related to the first-order derivatives $G_{ij}^{(1)}$ when $i=j$ can be acquired as below

$$G_{ii}^{(1)} = - \sum_{j=1, j \neq i}^{N_\phi} G_{ij}^{(1)}, \quad (15)$$

for $i=1, 2, 3, \dots, N_\phi$.

The weight coefficients related to the second-order derivatives $G_{ij}^{(2)}$ when $i \neq j$ would be acquired through the subsequent relation

$$G_{ij}^{(2)} = G_{ij}^{(1)} \left(2G_{ij}^{(1)} - \pi \cot\left(\frac{\phi_i - \phi_j}{2} \times \pi\right) \right), \quad (16)$$

$i, j = 1, 2, 3, \dots, N_\phi$.

The weight coefficients related to the second-order derivatives $G_{ii}^{(2)}$ when $i=j$ would be determined as

$$G_{ii}^{(2)} = - \sum_{j=1, j \neq i}^{N_\phi} G_{ij}^{(2)}, \quad (17)$$

for $i = 1, 2, 3, \dots, N_\phi$.

Also, the Chebyshev–Gauss–Lobatto grid distribution is chosen. In this distribution, the co-ordinates of grid points (\varnothing_i, θ_j) are calculated by the following equation across the reference surface.

The displacement field expressions are given as below,

$$\begin{aligned}
 T_0(\varnothing, \theta, t) &= R_1(\varnothing, \theta, t) = \\
 c_0(\varnothing, \theta) \exp(iLt), & a_1(\varnothing, \theta) \exp(iLt), \\
 S_1(\varnothing, \theta, t) &= T_1(\varnothing, \theta, t) = \\
 b_1(\varnothing, \theta) \exp(iLt), & c_1(\varnothing, \theta) \exp(iLt), \\
 R_2(\varnothing, \theta, t) &= S_2(\varnothing, \theta, t) = \\
 a_2(\varnothing, \theta) \exp(iLt), & b_2(\varnothing, \theta) \exp(iLt), \\
 T_2(\varnothing, \theta, t) &= R_3(\varnothing, \theta, t) = \\
 c_2(\varnothing, \theta) \exp(iLt), & a_3(\varnothing, \theta) \exp(iLt), \\
 S_3(\varnothing, \theta, t) &= T_3(\varnothing, \theta, t) = \\
 b_3(\varnothing, \theta) \exp(iLt), & c_3(\varnothing, \theta) \exp(iLt), \\
 R_4(\varnothing, \theta, t) &= S_4(\varnothing, \theta, t) = \\
 a_4(\varnothing, \theta) \exp(iLt), & b_4(\varnothing, \theta) \exp(iLt), \\
 T_4(\varnothing, \theta, t) &= R_5(\varnothing, \theta, t) = \\
 c_4(\varnothing, \theta) \exp(iLt), & a_5(\varnothing, \theta) \exp(iLt), \\
 S_5(\varnothing, \theta, t) &= T_5(\varnothing, \theta, t) = \\
 b_5(\varnothing, \theta) \exp(iLt), & = c_5(\varnothing, \theta) \exp(iLt).
 \end{aligned} \tag{18}$$

Using the above equations, the following linear set of equations are obtained:

$$\begin{aligned}
 & \left\{ \begin{bmatrix} [M_{dd}] & [M_{db}] \\ [M_{bd}] & [M_{bb}] \end{bmatrix} L^2 \right. \\
 & \left. + \begin{bmatrix} [K_{dd}] & [K_{db}] \\ [K_{bd}] & [K_{bb}] \end{bmatrix} \right\} \begin{Bmatrix} \mathcal{E}_d \\ \mathcal{E}_b \end{Bmatrix} = 0
 \end{aligned} \tag{19}$$

By solving Eq. (19), the natural frequency of the system can be achieved.

4. NUMERICAL RESULTS AND DISCUSSION

4.1. Material Properties

The material properties associated with GOPs reinforcement as well as concrete

matrix, and spherical vessel are presented in Table 1 adopted from Ref. (Z. Zhang et al., 2020).

Table 1. The properties of GOPs, polymer, and pressure vessel

Polymer epoxy(matrix)	Pressure vessel	GOPs
$v_m=0.42$	m_b (kg)=260	$v_{GOP}=0.165$
E_m (Mpa)=25	$\varnothing_j=10$ [deg]	ρ_{GOP} (kg/m ³)=1090
	$\varnothing_o=170$ [deg]	E_{GOP} (Gpa)=444.8
		d_{GOP} (nm)=500
		h_{GOP} (nm)=0.95

In addition the following dimensionless parameters are defined for natural frequency Ω and internal pressure \bar{P} :

$$\begin{aligned}
 \Omega &= \omega \frac{R^2}{h} \sqrt{\frac{\rho}{E}} \\
 \bar{P} &= \frac{P}{E_c}
 \end{aligned}$$

4.2. Validation

The new material and method presented in the current study need to be verified by comparing to the results of other studies in the similar structure and loading conditions. In this regard, the problem of vibrational behavior evaluation from Liu et al. (D. Liu, Zhou, & Zhu, 2021). The results are presented for two different parameter variation namely the mode number of vibration and the GOP distribution patterns. It is seen that the current method provides similar results to the selected reference which validate our methodology. On the other hand, different variation in pattern of GOP results in different natural frequency of pressure vessel shell structure which will be discussed in next sections in details along with several other parameters.

Table 2. Frequency parameter of the composite spherical shell

Mode number	Epoxy		GPL-UD		GPL-X		GPL-O	
	Ref. (D. Liu et al., 2021)	Present	Ref. (D. Liu et al., 2021)	Present	Ref. (D. Liu et al., 2021)	Present	Ref. (D. Liu et al., 2021)	Present
1	19.2432	19.2361	40.0892	40.0045	29.6019	29.5891	43.7133	43.6901
2	1.1613	1.1601	2.4194	2.4012	2.4203	2.4117	2.4196	2.4032
3	1.8362	1.8351	3.8253	3.8212	3.8263	3.8215	3.8251	3.8182
4	2.4635	2.4602	5.1322	5.1310	5.1324	5.1301	5.1309	5.1292

4.3. Parametric Study

This section examines the impact of different parameters and configurations on a nanocomposite shell of a pressure vessel. The number of layers within the nanocomposite structure plays a significant role in determining the natural frequency of the pressure vessel, as depicted in Figure 2. The figure illustrates that an increase in the number of layers, denoted as N_L , within the GOP-X configuration leads to a corresponding increase in the natural frequency of the structure, particularly for a low number of layers. However, for a higher number of layers ($N_L > 50$), an increase in the number of layers has minimal effect on the natural frequency, assuming all other parameters remain constant. In contrast, an increase in the number of layers in the GOP-O configuration has the opposite effect on the natural frequency of the pressure vessel structures. Specifically, as the number of layers in GOP-O increases, the natural frequency decreases. On the other hand, altering the number of layers in the uniform configuration does not have any influence on the natural frequency of the structure. Therefore, this analysis demonstrates the significant influence of the number of layers and different configurations on the natural frequency of nanocomposite shell structures, with distinct behaviors observed for different configurations.

Table 3. Effects of number of layers and distribution pattern of GOP on the dimensionless frequency of concrete pressure vessel

N_L	GOP-X	GOP-U	GOP-O
7	0.6309	0.6309	0.6310
9	0.6311	0.6309	0.6308
11	0.6312	0.6309	0.6307
13	0.6312	0.6309	0.6307
15	0.6312	0.6309	0.6307
25	0.6313	0.6309	0.6306
35	0.6313	0.6309	0.6306
55	0.6313	0.6309	0.6306
100	0.6313	0.6309	0.6306

The natural frequency of the shell is influenced by an increase in the thickness of the structure (h) in comparison to the radius of the pressure vessel (r), as illustrated in Figure 2. This analysis considers various weight fractions of GOP (W_{GOP}). The figure demonstrates that an increase in the thickness of the pressure vessel shell leads to a corresponding increase in the natural frequency of the structure, regardless of the weight fraction of GOP. This effect is expected, as increasing the thickness while keeping the radius constant results in a higher stiffness within the structure, ultimately raising its natural frequency. Furthermore, an increase in the weight fraction of GOP contributes to an increase in the stiffness of the structure, consequently

elevating the natural frequency. This relationship is consistent with the expectation that higher weight fractions of GOP enhance the overall stiffness of the nanocomposite shell. Therefore, both an increase in the thickness of the structure relative to the pressure vessel radius and an increase in the weight fraction of GOP lead to an increase in the natural frequency of the structure. These findings align with the anticipated effects of stiffness enhancement resulting from changes in the structural parameters and the incorporation of GOP within the nanocomposite shell.

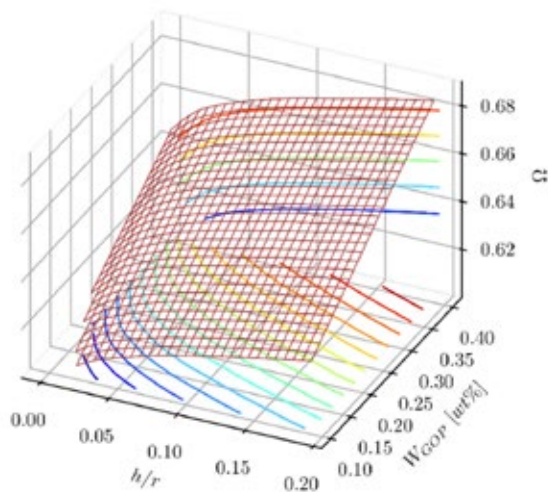


Figure 2. Effect of h/r aspect ratio and W_{GOP} on the natural frequency of pressure vessel

The natural frequency of the entire shell model is also influenced by the total mass of the spherical vessel, as shown in Figure 3 for various thicknesses. An increase in the mass of the pressure vessel, while keeping the geometrical parameters constant, corresponds to a decrease in the material density. This decrease in density results in a reduction in the natural frequency of the structure, as can be observed from the curves in Figure 4. Similarly, the effect of the h/r aspect ratio (the ratio of thickness to radius) on the natural frequency follows a similar trend to that depicted in Figure 2. As the h/r aspect ratio increases, there is a corresponding increase in the natural frequency of the shell structure.

Therefore, the total mass of the spherical vessel and the h/r aspect ratio play significant roles in determining the natural frequency of the entire shell model. Increasing the mass, which decreases the material density, results in a decrease in the natural frequency. Additionally, an increase in the h/r aspect ratio leads to an increase in the natural frequency, highlighting the influence of structural dimensions on the dynamic characteristics of the shell.

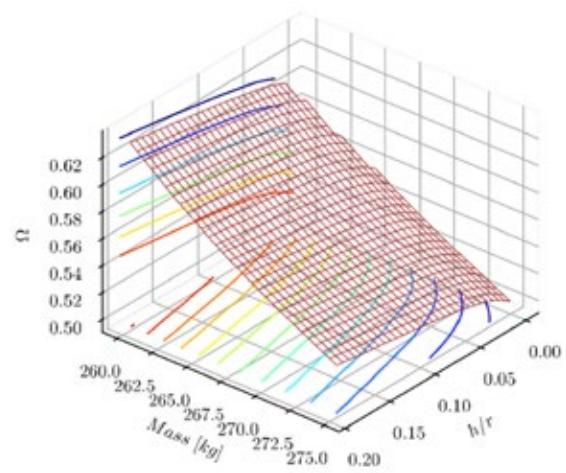


Figure 3. Effect of total mass of the pressure vessel m_b and h/r on the natural frequency of pressure vessel

An increase in the angle ϕ generally leads to a decrease in the natural frequency of the structure for all thickness values, as illustrated in Figure 4. However, the extent of this decrease varies depending on the specific thickness and the value of the angle ϕ . In cases with low angles, it is observed that the natural frequency experiences a more significant increase compared to other angle values. The gradient of increase in the natural frequency is higher for lower angle values. This implies that small changes in the angle ϕ at lower angles have a more pronounced effect on reducing the natural frequency of the structure. Conversely, as the angle ϕ increases, the decrease in the natural frequency becomes less pronounced. The influence of the angle ϕ on the natural frequency is still present, but the effect is relatively milder compared to lower angle values.

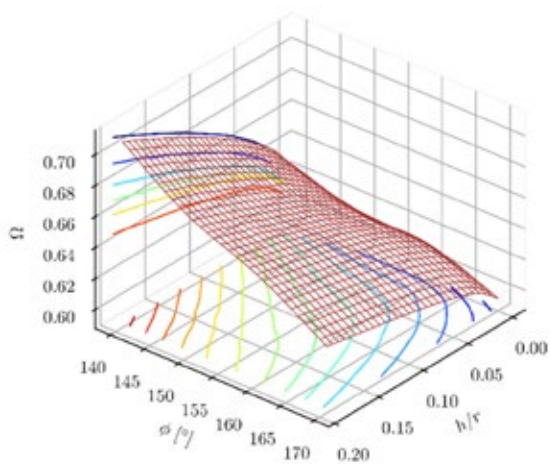


Figure 4. Effect of angle ϕ and h/r on the natural frequency of pressure vessel

The boundary condition plays a crucial role in determining the natural frequency of the structure, as shown in Table 4. By altering the boundary condition, the natural frequency of the structure varies across different values of the h/r (thickness to radius) ratio.

Among the different boundary conditions considered, the simply supported boundary condition results in the smallest natural frequency for a constant value of the h/r ratio. This indicates that the structure exhibits a lower frequency response when it is supported at the ends, allowing for some degree of freedom in terms of displacement.

On the other hand, the clamped boundary condition corresponds to the highest frequency values. This boundary condition restricts the structure from experiencing any displacement at the ends, leading to a higher stiffness and consequently a higher natural frequency.

These findings demonstrate that the state of the boundary condition is a determining factor in calculating the natural frequency of the structure. Different boundary conditions result in varying natural frequency values, with the simply supported condition yielding the lowest frequency and the clamped condition producing the highest frequency.

In the previous parametric studies, it was assumed that the internal pressure of the

pressure vessel is equal to the ambient pressure. However, in reality, the pressure inside the pressure vessel is positive. The variation in the internal pressure of the pressure vessel has a significant impact on the natural frequency of the structure, as illustrated in Figure 5.

Table 4. Effects of h/r and type of boundary condition on the dimensionless frequency of concrete pressure vessel

h/r	S-S	C-S	C-C
0	0.55942	0.57244	0.59619
0.05	0.57459	0.58809	0.61280
0.1	0.58263	0.59646	0.62015
0.15	0.58848	0.60291	0.62601
0.2	0.59315	0.60840	0.63128

The figure reveals that changing the parameter \bar{P} from positive values to negative values substantially alters the behavior of the frequency curves. When the parameter \bar{P} has positive or zero values, the natural frequency monotonically increases for all values of the h/r ratio. This implies that as the internal pressure increases, the natural frequency of the structure also increases.

However, in the case of negative values of parameter \bar{P} , the behavior of the natural frequency changes. For lower values of the h/r ratio, the natural frequency decreases as the h/r ratio increases. This implies that the internal pressure has a counterintuitive effect on the natural frequency for certain values of the h/r ratio.

In each value of parameter \bar{P} , there is a turning point in the curves where the natural frequency begins to rise. This indicates that there is a critical value of the h/r ratio at which the influence of the internal pressure on the natural frequency changes. Interestingly, all the curves converge and coincide at a high value of the h/r ratio. This suggests that at sufficiently large values of the h/r ratio, the influence of the internal pressure becomes negligible, and the natural frequency reaches a steady state. The vari-

ation in the internal pressure of the pressure vessel has a profound impact on the natural frequency of the structure. Positive and zero values of the internal pressure lead to a monotonic increase in the natural frequency, while negative values introduce complex behavior, with a turning point and counterintuitive effects for certain h/r ratios. The curves ultimately converge and coincide at high h/r ratios, indicating the diminishing influence of the internal pressure.

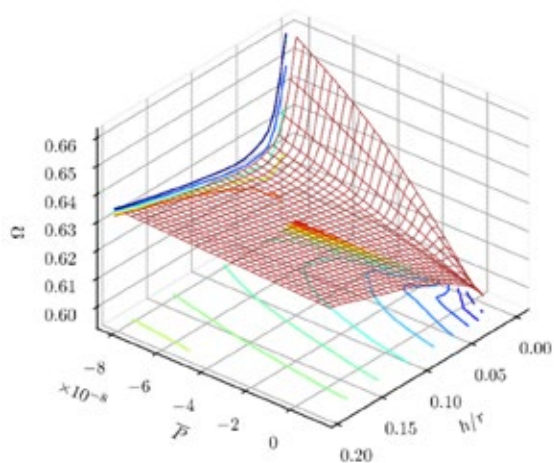


Figure 5. Effect of parameter P and h/r on the natural frequency of pressure vessel

Figure 6 illustrates the simultaneous effects of the h/r aspect ratio and the weight fraction of GOP on the natural frequency of the structure. Similar to Figure 2, an increase in both of these parameters leads to an increase in the natural frequency of the structure. However, one notable feature of the present graph is the semi-linear change in the natural frequency due to variations in the weight fraction of the GOP, which was not apparent from Figure 2.

The graph demonstrates that as the h/r aspect ratio increases, there is a corresponding increase in the natural frequency for various weight fractions of GOP. This relationship is consistent with the understanding that a larger h/r ratio results in a stiffer structure, leading to higher natural frequencies.

Furthermore, the weight fraction of the GOP has a distinct effect on the natural

frequency. In Figure 6, it is observed that as the weight fraction of GOP increases, the natural frequency also increases. However, unlike in Figure 2, where the relationship between weight fraction and natural frequency appeared to be linear, Figure 6 reveals a semi-linear change in the natural frequency. This suggests that the influence of the weight fraction of GOP on the natural frequency is more nuanced and exhibits a gradual change as the weight fraction varies.

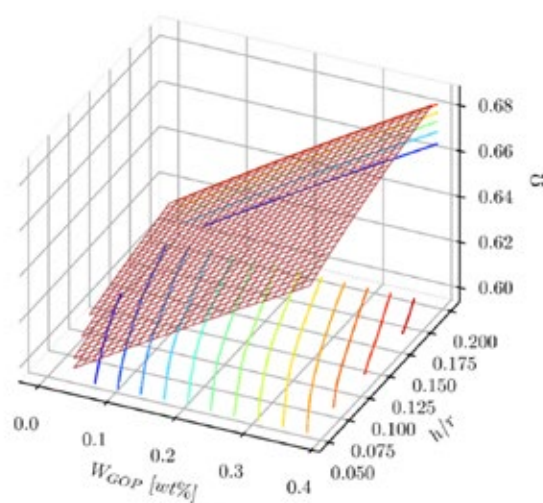


Figure 6. Effect of W_{GOP} and h/r on the natural frequency of pressure vessel

In Figure 7, the linear increase of the natural frequency with an increase in the weight fraction of GOP is observed, similar to the previous findings. This indicates that as the weight fraction of GOP increases, the natural frequency of the structure also increases in a linear fashion. Additionally, the effect of pressure vessel mass on the natural frequency is evident in Figure 7. Higher values of pressure vessel mass correspond to lower values of the natural frequency. This means that as the mass of the pressure vessel increases, the natural frequency of the structure decreases. The relationship between pressure vessel mass and natural frequency can be attributed to the increased inertia of the structure caused by the higher mass. The higher mass contributes to a greater resistance against displacement and thus results in a lower natural frequency.

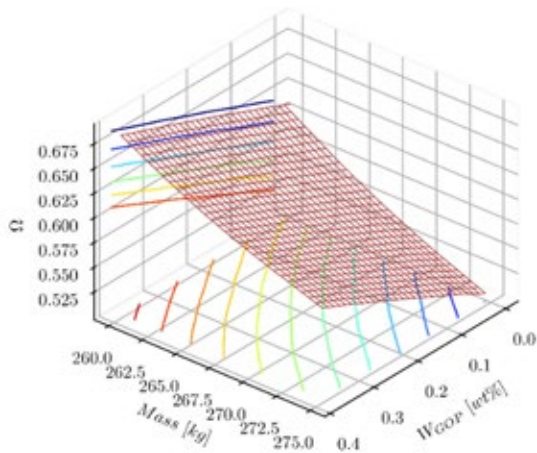


Figure 7. Effect of total mass of the pressure vessel m_b and W_{GOP} on the natural frequency of pressure vessel

Figure 8 illustrates the simultaneous effects of the angle ϕ and the weight fraction of GOP (Graphene Oxide Polymer) on the natural frequency of the structure. As observed in Figure 2, an increase in the weight fraction (W_{GOP}) leads to an increase in the natural frequency of the structure.

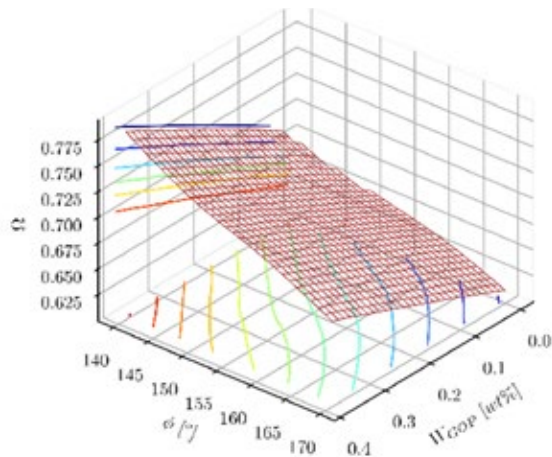


Figure 8. Effect of angle ϕ_0 and W_{GOP} on the natural frequency of pressure vessel

However, an important feature depicted in Figure 8 is the decrease in the natural frequency of the structure with an increase in the angle ϕ from 140° to 170° . This observation contrasts with the general trend seen in the previous figures. The decrease in the natural frequency with an increase in the angle ϕ suggests that certain angular configurations have a dampening effect on the dynamic response of the structure. This behavior may be attributed to

the specific geometry and material properties associated with the angle ϕ range of 140° to 170° . It is worth noting that this unique feature was not evident in Figure 2, indicating that the interaction between the angle ϕ and the weight fraction of GOP introduces additional complexities to the natural frequency response.

5. CONCLUSION

This paper presents a comprehensive investigation on the vibrations of spherical concrete pressure vessels reinforced by graphene oxide powders (GOPs) using a polynomial displacement field and the Generalized Differential Quadrature Method (GDQM). This research contributes to advancing the understanding of the vibrational behavior of graphene oxide-reinforced spherical concrete pressure vessels, particularly focusing on the influence of different distribution patterns of GOPs. The findings offer valuable insights for engineers and researchers involved in the design and analysis of pressure vessels, contributing to improved structural integrity and performance. The main results could be given in the following items:

- Firstly, it is observed that higher pressure vessel masses result in lower natural frequencies. This is due to the increased mass, which contributes to higher inertia and stiffness, thus reducing the natural frequency of the structure.
- Secondly, variations in the internal pressure of the pressure vessel have a significant influence on its natural frequency. Changes in internal pressure directly affect the structural dynamics, leading to variations in the natural frequency.
- Additionally, an increase in the thickness of the pressure vessel shell is found to cause an increase in the natural frequency. This is attributed to the higher stiffness resulting from

the thicker shell, leading to a higher natural frequency of vibration.

- Furthermore, the weight fraction of GOP demonstrates a linear relationship with the natural frequency. Increasing the weight fraction proportionally increases the natural frequency, indicating that the addition of GOP enhances the overall stiffness and dynamic characteristics of the pressure vessel.

6. REFERENCES

- Al-Furjan, M. S. H., Habibi, M., Jung, D. w., Sadeghi, S., Safarpour, H., Tounsi, A., & Chen, G. (2022). A computational framework for propagated waves in a sandwich doubly curved nanocomposite panel. *Engineering with Computers*, 38(2), 1679-1696. doi:<https://doi.org/10.1007/s00366-020-01130-8>
- Al-Furjan, M. S. H., Oyarhossein, M. A., Habibi, M., Safarpour, H., & Jung, D. W. (2020). Wave propagation simulation in an electrically open shell reinforced with multiphase nanocomposites. *Engineering with Computers*. doi:<https://doi.org/10.1007/s00366-020-01167-9>
- Chen, Y. Z., & Lin, X. Y. (2008). Elastic analysis for thick cylinders and spherical pressure vessels made of functionally graded materials. *Computational Materials Science*, 44(2), 581-587. doi:<https://doi.org/10.1016/j.commatsci.2008.04.018>
- Cong, S., Cheng, Z., Tang, L., & Ling, X. (2023). Fatigue properties and microstructure of graphene oxide/microcapsule self-healing concrete. *Journal of Building Engineering*, 70, 106264. doi:<https://doi.org/10.1016/j.jobe.2023.106264>
- Dai, Z., Jiang, Z., Zhang, L., & Habibi, M. (2021). Frequency characteristics and sensitivity analysis of a size-dependent laminated nanoshell. *Advances in nano research*, 10(2), 175. doi:<https://doi.org/10.12989/anr.2021.10.2.175>
- Dong, Q., Li, Q. M., & Zheng, J. Y. (2010). Interactive mechanisms between the internal blast loading and the dynamic elastic response of spherical containment vessels. *International Journal of Impact Engineering*, 37(4), 349-358. doi:<https://doi.org/10.1016/j.ijimpeng.2009.10.004>
- Ebrahimi, F., Hajilak, Z. E., Habibi, M., & Safarpour, H. (2019). Buckling and vibration characteristics of a carbon nanotube-reinforced spinning cantilever cylindrical 3D shell conveying viscous fluid flow and carrying spring-mass systems under various temperature distributions. *Proceedings of the Institution of Mechanical Engineers, Part C: Journal of Mechanical Engineering Science*, 233(13), 4590-4605. doi:<https://doi.org/10.1177/0954406219832323>
- Ebrahimi, F., Mohammadi, K., Barouti, M. M., & Habibi, M. (2019). Wave propagation analysis of a spinning porous graphene nanoplatelet-reinforced nanoshell. *Waves in Random and Complex Media*, 1-27. doi:<https://doi.org/10.1080/17455030.2019.1694729>
- Ebrahimi, F., Supeni, E. E. B., Habibi, M., & Safarpour, H. (2020). Frequency characteristics of a GPL-reinforced composite microdisk coupled with a piezoelectric layer. *The European Physical Journal Plus*, 135(2), 144. doi:<https://doi.org/10.1140/epjp/s13360-020-00217-x>
- Ghavanloo, E., Rafii-Tabar, H., & Fazelzadeh, S. A. (2019). New insights on nonlocal spherical shell model and its application to free vibration of spherical fullerene molecules. *International Journal of Mechanical Sciences*, 161-162, 105046. doi:<https://doi.org/10.1016/j.ijmecsci.2019.105046>
- Godoy, L. A. (1987). A simplified bending analysis of imperfect spherical pressure vessels. *International Journal of Pres-*

sure Vessels and Piping, 27(5), 385-399. doi:[https://doi.org/10.1016/0308-0161\(87\)90059-7](https://doi.org/10.1016/0308-0161(87)90059-7)

Guo, J., Baharvand, A., Tazeddinova, D., Habibi, M., Safarpour, H., Roco-Videla, A., & Selmi, A. (2021). An intelligent computer method for vibration responses of the spinning multi-layer symmetric nanosystem using multi-physics modeling. *Engineering with Computers*, 1-22. doi:<https://doi.org/10.1007/s00366-021-01433-4>

Habibi, M., Mohammadi, A., Safarpour, H., Shavalipour, A., & Ghadiri, M. (2021). Wave propagation analysis of the laminated cylindrical nanoshell coupled with a piezoelectric actuator. *Mechanics Based Design of Structures and Machines*, 49(5), 640-658.

Habibi, M., Safarpour, M., & Safarpour, H. (2020). Vibrational characteristics of a FG-GPLRC viscoelastic thick annular plate using fourth-order Runge-Kutta and GDQ methods. *Mechanics Based Design of Structures and Machines*, 1-22. doi:<https://doi.org/10.1080/15397734.2020.1779086>

Hamed, E., Bradford, M. A., & Ian Gilbert, R. (2010). Nonlinear long-term behaviour of spherical shallow thin-walled concrete shells of revolution. *International Journal of Solids and Structures*, 47(2), 204-215. doi:<https://doi.org/10.1016/j.ijsolstr.2009.09.027>

Hashemi, H. R., Alizadeh, A. a., Oyarhossein, M. A., Shavalipour, A., Makkiabadi, M., & Habibi, M. (2019). Influence of imperfection on amplitude and resonance frequency of a reinforcement compositionally graded nanostructure. *Waves in Random and Complex Media*, 1-27. doi:<https://doi.org/10.1080/17455030.2019.1662968>

Hutchinson, J. W. (2016). Buckling of spherical shells revisited. *Proceedings of the Royal Society A: Mathematical, Physical and Engineering Sciences*, 472(2195), 20160577.

doi:<https://doi.org/10.1098/rspa.2016.0577>

Hwangbo, D., Son, D.-H., Suh, H., Sung, J., Bae, B.-I., Bae, S., Choi, C.-S. (2023). Effect of nanomaterials (carbon nanotubes, nanosilica, graphene oxide) on bond behavior between concrete and reinforcing bars. *Case Studies in Construction Materials*, 18, e02206. doi:<https://doi.org/10.1016/j.cscm.2023.e02206>

Jaramillo, L. J., & Kalfat, R. (2023). Fresh and hardened performance of concrete enhanced with graphene nanoplatelets (GNPs). *Journal of Building Engineering*, 75, 106945. doi:<https://doi.org/10.1016/j.jobbe.2023.106945>

Kong, F., Dong, F., Duan, M., Habibi, M., Safarpour, H., & Tounsi, A. (2022). On the vibrations of the Electrorheological sandwich disk with composite face sheets considering pre and post-yield regions. *Thin-Walled Structures*, 179, 109631. doi:<https://doi.org/10.1016/j.tws.2022.109631>

Lee, H.-S., Yoon, J.-H., Park, J.-S., & Yi, Y.-M. (2005). A study on failure characteristic of spherical pressure vessel. *Journal of Materials Processing Technology*, 164-165, 882-888. doi:<https://doi.org/10.1016/j.jmatprotec.2005.02.208>

Liu, D., Zhou, Y., & Zhu, J. (2021). On the free vibration and bending analysis of functionally graded nanocomposite spherical shells reinforced with graphene nanoplatelets: Three-dimensional elasticity solutions. *Engineering Structures*, 226, 111376. doi:<https://doi.org/10.1016/j.engstruct.2020.111376>

Liu, Z., Su, S., Xi, D., & Habibi, M. (2020). Vibrational responses of a MHC viscoelastic thick annular plate in thermal environment using GDQ method. *Mechanics Based Design of Structures and Machines*, 1-26. doi:<https://doi.org/10.1080/15397734.2020.1784201>

Lu, L., Liao, K., Habibi, M., Safarpour, H., & Ali, H. E. (2023). *Numerical methods to predict aero thermally induced vibrations of a curved pipe structure reinforced by GPLs*. Paper presented at the Structures.

Lu, S., Li, S., Habibi, M., & Safarpour, H. (2023). Improving the thermo-electro-mechanical responses of MEMS resonant accelerometers via a novel multi-layer perceptron neural network. *Measurement*, 113168. doi:<https://doi.org/10.1016/j.measurement.2023.113168>

Ma, B., Chen, K.-y., Habibi, M., & Albaijan, I. (2023). Static/dynamic analyses of sandwich micro-plate based on modified strain gradient theory. *Mechanics of Advanced Materials and Structures*, 1-8. doi:<https://doi.org/10.1080/15376494.2023.2219453>

Mahapatra, T. R., Kar, V. R., & Panda, S. K. (2015). Large Amplitude Vibration Analysis of Laminated Composite Spherical Panels Under Hygrothermal Environment. *International Journal of Structural Stability and Dynamics*, 16(03), 1450105. doi:<https://doi.org/10.1142/S0219455414501053>

Moayedi, H., Aliakbarlou, H., Jebeli, M., Noormohammadiarani, O., Habibi, M., Safarpour, H., & Foong, L. (2020). Thermal buckling responses of a graphene reinforced composite micropanel structure. *International Journal of Applied Mechanics*, 12(01), 2050010. doi:<https://doi.org/10.1142/S1758825120500106>

Moayedi, H., Aliakbarlou, H., Jebeli, M., Noormohammadiarani, O., Habibi, M., Safarpour, H., & Foong, L. K. (2020). Thermal Buckling Responses of a Graphene Reinforced Composite Micropanel Structure. *International Journal of Applied Mechanics*, 12(01), 2050010. doi:<https://doi.org/10.1142/S1758825120500106>

Moayedi, H., Ebrahimi, F., Habibi, M., Safarpour, H., & Foong, L. K. (2020). Application of nonlocal strain–stress gradient theory and GDQEM for thermo-vibra-

tion responses of a laminated composite nanoshell. *Engineering with Computers*, 1-16. doi:<https://doi.org/10.1007/s00366-020-01002-1>

Moayedi, H., Habibi, M., Safarpour, H., Safarpour, M., & Foong, L. (2019). Buckling and frequency responses of a graphene nanoplatelet reinforced composite microdisk. *International Journal of Applied Mechanics*, 11(10), 1950102. doi:<https://doi.org/10.1142/S1758825119501023>

Mohammadgholiha, M., Shokrgozar, A., Habibi, M., & Safarpour, H. (2019). Buckling and frequency analysis of the nonlocal strain–stress gradient shell reinforced with graphene nanoplatelets. *Journal of Vibration and Control*, 25(19-20), 2627-2640. doi:<https://doi.org/10.1177/1077546319863251>

Mohammadi, A., Lashini, H., Habibi, M., & Safarpour, H. (2019). Influence of viscoelastic foundation on dynamic behaviour of the double walled cylindrical inhomogeneous micro shell using MCST and with the aid of GDQM. *Journal of Solid Mechanics*, 11(2), 440-453. doi:10.22034/JSM.2019.665264

Oyarhossein, M. A., Alizadeh, A. a., Habibi, M., Makkiabadi, M., Daman, M., Safarpour, H., & Jung, D. W. (2020). Dynamic response of the nonlocal strain-stress gradient in laminated polymer composites microtubes. *Scientific reports*, 10(1), 1-19. doi:<https://doi.org/10.1038/s41598-020-61855-w>

Pan, B., & Cui, W. (2010). An overview of buckling and ultimate strength of spherical pressure hull under external pressure. *Marine Structures*, 23(3), 227-240. doi:<https://doi.org/10.1016/j.marstruc.2010.07.005>

Pang, F., Li, H., Chen, H., & Shan, Y. (2021). Free vibration analysis of combined composite laminated cylindrical and spherical shells with arbitrary boundary conditions. *Mechanics of Advanced Materials and Structures*

tures, 28(2), 182-199. doi:<https://doi.org/10.1080/15376494.2018.1553258>

Sajjad, U., Sheikh, M. N., & Hadi, M. N. S. (2022). Incorporation of graphene in slag-fly ash-based alkali-activated concrete. *Construction and Building Materials*, 322, 126417. doi:<https://doi.org/10.1016/j.conbuildmat.2022.126417>

Shahpari, M., Bamonte, P., & Jalali Mossallam, S. (2022). An experimental study on mechanical and thermal properties of structural lightweight concrete using carbon nanotubes (CNTs) and LECA aggregates after exposure to elevated temperature. *Construction and Building Materials*, 346, 128376. doi:<https://doi.org/10.1016/j.conbuildmat.2022.128376>

Shao, Y., Zhao, Y., Gao, J., & Habibi, M. (2021). Energy absorption of the strengthened viscoelastic multi-curved composite panel under friction force. *Archives of Civil and Mechanical Engineering*, 21(4), 1-29. doi:<https://doi.org/10.1007/s43452-021-00279-3>

Shariati, A., Habibi, M., Tounsi, A., Safarpour, H., & Safa, M. (2020). Application of exact continuum size-dependent theory for stability and frequency analysis of a curved cantilevered microtubule by considering viscoelastic properties. *Engineering with Computers*, 1-20. doi:<https://doi.org/10.1007/s00366-020-01024-9>

Shariati, A., Mohammad-Sedighi, H., Żur, K. K., Habibi, M., & Safa, M. (2020). On the vibrations and stability of moving viscoelastic axially functionally graded nanobeams. *Materials*, 13(7), 1707. doi:<https://doi.org/10.3390/ma13071707>

Shokrgozar, A., Safarpour, H., & Habibi, M. (2020). Influence of system parameters on buckling and frequency analysis of a spinning cantilever cylindrical 3D shell coupled with piezoelectric actuator. *Proceedings of the Institution of Mechanical Engineers, Part C: Journal of Mechanical Engineering Sci-*

ence, 234(2), 512-529. doi:<https://doi.org/10.1177/0954406219883312>

Siahkouhi, M., Razaqpur, G., Hoult, N. A., Hajmohammadian Baghban, M., & Jing, G. (2021). Utilization of carbon nanotubes (CNTs) in concrete for structural health monitoring (SHM) purposes: A review. *Construction and Building Materials*, 309, 125137. doi:<https://doi.org/10.1016/j.conbuildmat.2021.125137>

Tang, J., Wu, S., Habibi, M., Safarpour, M., & Ali, H. E. (2023). Flutter analysis of multi-directional functionally graded sector poroelastic disks. *Aerospace Science and Technology*, 140, 108481. doi:<https://doi.org/10.1016/j.ast.2023.108481>

Van Do, V. N., & Lee, C.-H. (2020). Static bending and free vibration analysis of multilayered composite cylindrical and spherical panels reinforced with graphene platelets by using isogeometric analysis method. *Engineering Structures*, 215, 110682. doi:<https://doi.org/10.1016/j.engstruct.2020.110682>

Wang, Y., Jia, Q., Deng, T., Habibi, M., Al-Kikani, S., & Ali, H. E. (2023). Wave propagation analysis of the ball in the handball's game. *Structural Engineering and Mechanics*, 85(6), 729-742.

Wang, Z., Yu, S., Xiao, Z., & Habibi, M. (2020). Frequency and buckling responses of a high-speed rotating fiber metal laminated cantilevered microdisk. *Mechanics of Advanced Materials and Structures*, 1-14. doi:<https://doi.org/10.1080/15376494.2020.1824284>

Wu, J., & Habibi, M. (2021). Dynamic simulation of the ultra-fast-rotating sandwich cantilever disk via finite element and semi-numerical methods. *Engineering with Computers*, 1-17. doi:<https://doi.org/10.1007/s00366-021-01396-6>

Yan, C., Wang, Y., Zhai, X., Meng, L., & Zhou, H. (2019). Experimental study on curved steel-concrete-steel sandwich

shells under concentrated load by a hemispherical head. *Thin-Walled Structures*, 137, 117-128. doi:<https://doi.org/10.1016/j.tws.2019.01.007>

Yue, H., Hua, S., Qian, H., Yao, X., Gao, Y., & Jiang, F. (2022). Investigation on applicability of spherical electric arc furnace slag as fine aggregate in superplasticizer-free 3D printed concrete. *Construction and Building Materials*, 319, 126104. doi:<https://doi.org/10.1016/j.conbuildmat.2021.126104>

Zeng, H., Qu, S., Tian, Y., Hu, Y., & Li, Y. (2023). Recent progress on graphene oxide for next-generation concrete: Characterizations, applications and challenges. *Journal of Building Engineering*, 69, 106192. doi:<https://doi.org/10.1016/j.jobe.2023.106192>

Zhang, J., Zhang, M., Cui, W., Tang, W., Wang, F., & Pan, B. (2018). Elastic-plastic buckling of deep sea spheri-

cal pressure hulls. *Marine Structures*, 57, 38-51. doi:<https://doi.org/10.1016/j.marstruc.2017.09.007>

Zhang, Z., Li, Y., Wu, H., Zhang, H., Wu, H., Jiang, S., & Chai, G. (2020). Mechanical analysis of functionally graded graphene oxide-reinforced composite beams based on the first-order shear deformation theory. *Mechanics of Advanced Materials and Structures*, 27(1), 3-11. doi:<https://doi.org/10.1080/15376494.2018.1444216>

Zhou, C., Zhao, Y., Zhang, J., Fang, Y., & Habibi, M. (2020). Vibrational characteristics of multi-phase nanocomposite reinforced circular/annular system. *Advances in nano research*, 9(4), 295-307. doi:<https://doi.org/10.12989/anr.2020.9.4.295>

Zingoni, A. (2022). Stress and buckling resistance of dual-purpose concrete shells. *Thin-Walled Structures*, 170, 108596. doi:<https://doi.org/10.1016/j.tws.2021.108596>